Journal of Biomedical Optics

BiomedicalOptics.SPIEDigitalLibrary.org

Imaging microscopic distribution of antifungal agents in dandruff treatments with stimulated Raman scattering microscopy

Natalie L. Garrett
Bhumika Singh
Andrew Jones
Julian Moger

SPIE.

Natalie L. Garrett, Bhumika Singh, Andrew Jones, Julian Moger, "Imaging microscopic distribution of antifungal agents in dandruff treatments with stimulated Raman scattering microscopy," *J. Biomed. Opt.* **22**(6), 066003 (2017), doi: 10.1117/1.JBO.22.6.066003.

Journal of Biomedical Optics 22(6), 066003 (June 2017)

Imaging microscopic distribution of antifungal agents in dandruff treatments with stimulated Raman scattering microscopy

Natalie L. Garrett,[a] Bhumika Singh,[b] Andrew Jones,[b] and Julian Moger[a,*]
[a]University of Exeter, School of Physics, Exeter, Devon, United Kingdom
[b]Unilever Research and Development, Port Sunlight, Bebington, United Kingdom

Abstract. Treatment of dandruff condition usually involves use of antidandruff shampoos containing antifungal agents. Different antifungal agents show variable clinical efficacy based on their cutaneous distribution and bioavailability. Using stimulated Raman scattering (SRS), we mapped the distribution of unlabeled low-molecular weight antifungal compounds zinc pyrithione (ZnPT) and climbazole (CBZ) on the surface of intact porcine skin with cellular precision. SRS has sufficient chemical selectivity and sensitivity to detect the agents on the skin surface based on their unique chemical motifs that do not occur naturally in biological tissues. Moreover, SRS is able to correlate the distribution of the agents with the morphological features of the skin using the CH_2 stretch mode, which is abundant in skin lipids. This is a significant strength of the technique since it allows the microscopic accumulation of the agents to be correlated with physiological features and their chemical environment without the use of counter stains. Our findings show that due to its lower solubility, ZnPT coats the surface of the skin with a sparse layer of crystals in the size range of 1 to 4 μm. This is consistent with the current understanding of the mode of action of ZnPT. In contrast, CBZ being more soluble and hydrophobic resulted in diffuse homogeneous distribution. It predominantly resided in microscopic lipid-rich crevasses and penetrated up to 60 μm into the infundibular spaces surrounding the hair shaft. The ability of the SRS to selectively map the distribution of agents on the skin's surface has the potential to provide insight into the mechanisms underpinning the topical application of antifungal or skin-active agents that could lead to the rational engineering of enhanced formulations. [DOI: 10.1117/1.JBO.22.6.066003]

Keywords: coherent Raman scattering; nonlinear optical spectroscopy; nonlinear optical microscopy; dermatology; antifungal.

Paper 170185R received Mar. 27, 2017; accepted for publication May 22, 2017; published online Jun. 9, 2017.

1 Introduction

Fungal skin conditions such as dandruff are caused by numerous host factors in conjunction with the skin flora yeast *Malassezia*.[1] Clinical studies have shown that topical administration of antifungal agents leads to an improvement in the condition,[2] and most commercially available antidandruff shampoo formulations include antifungal agents as the main active ingredients.

Comparative studies have reported great variation (up to 100-fold differences) in the efficacy of different antidandruff formulations in commercial shampoos, with the efficacy of different antifungal active ingredients (AIs) showing very different dependences on the concentration.[3] Fully understanding the dose response of different antifungal agents and rationally engineering more effective antifungal formulations requires new insight into how the physicochemical properties of different antifungal agents relate to their ability to penetrate into the microscopic features on the skin surface where fungal cells reside.

Macroscopically, skin is a uniform barrier against invasion from pathogens, chemical and physical assaults, and the unregulated loss of water and solutes. On the microscopic scale, skin is a complex heterogeneous structure with micron-scale features, such as hair follicles and pores, that perform vital physiological functions. Skin comprises three main layers (see Fig. 1): the epidermis, the outer layer containing keratinocytes, melanocytes, and corneocytes; the dermis, a middle region containing connective tissue, fibroblasts, immune cells, and hair follicles, as well as sebaceous and sweat glands; and the subcutaneous layer, the deepest layer, which is composed of connective tissue and fat. The outermost layer of the epidermis is known as the stratum corneum (SC), a cornified layer comprised of flattened, dead skin cells that is continually being shed and regenerated by cells pushing up from deeper within the SC. The microscopic topography of the skin contains features that harbor fungal cells, and, due to their different chemical environments, these features have varying accessibility to AIs with different physicochemical properties. Hair follicles are sheaths of cells and connective tissue surrounding hair roots and are composed of three segments: the upper segment (infundibulum), the middle segment (isthmus), and the lower segment (bulb and suprabulb). The infundibular space acts as a channel for the sebaceous gland's oily secretions, allowing them to be deposited onto the skin's surface. These secretions are mainly composed of wax esters, squalene, and triglycerides and form a crucial part of the skin's "acid mantle," which is a thin film of sebum, corneocyte debris, and residual materials from sweat.[4] The acid mantle's thickness varies depending on the topography of the skin; it settles into furrows and thus is microscopically thicker in regions with wrinkles and dermatoglyphs.

Antifungal agents are only effective if they reach pathogens at efficacious concentrations. However, application of an

*Address all correspondence to: Julian Moger, E-mail: j.moger@exeter.ac.uk

1083-3668/2017/$25.00

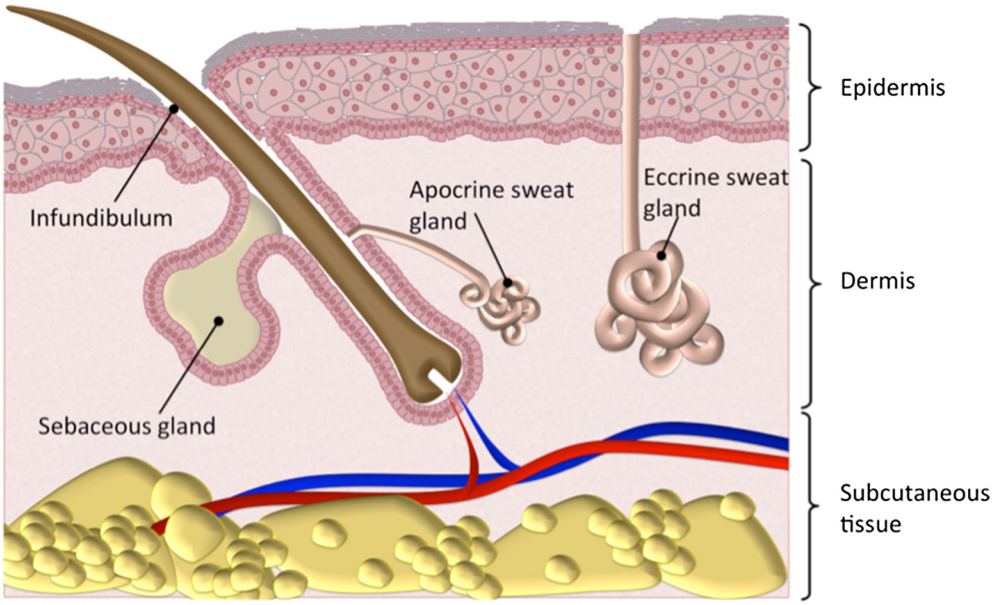

Fig. 1 Schematic cross-section of the skin, illustrating the structures found within the epidermis, dermis, and subcutaneous tissues, including the hair shaft and follicle, the apocrine and eccrine sweat glands, and the sebaceous gland. The epidermis comprises the horny barrier of the SC (on the surface), followed by the stratum lucidum, stratum granulosum, stratum spinosum, and SB.

antidandruff formulation over the surface of the skin at the required concentration does not necessarily result in equal delivery of active ingredients to the microscopic features of the skin surface. Different microscopic chemical environments (i.e., aqueous versus lipidic) affect the accessibility of the antifungal agents depending on their physicochemical properties within the formulation. This may sometimes result in a heterogeneous distribution that can lead to insufficient dosage to areas with an accumulation of fungi. For example, hair follicles are known to harbor *Malassezia*[5,6] and are particularly challenging sites to deliver water-soluble agents due to the lipid-rich environment surrounding the hair shaft.

Current clinical studies provide insightful information on the effectiveness of antidandruff formulations.[7] It would also be valuable to take into account how the concentration of different agents at different microscopic sites within the skin influences the clinical observations. The capability to correlate the efficacy of antifungals with their ability to reach specific target sites would lead to the rational engineering of enhanced formulations; however, this requires new methodologies to map the distribution of compounds at the microscopic scale on the skin surface.

The most widespread method for determining the delivery of topically applied formulations as a function of depth into the SC involves tape stripping. In this technique, a layer of adhesive film is pressed onto the skin and removed, weighed, and subjected to analysis to determine the relative composition of SC and applied formulations. However, despite providing a quantitative estimate of concentration as a function of depth,[8,9] this technique provides no spatial information regarding the microscopic location of agents. Cyanoacrylate tape stripping of the scalp skin has proved useful in three-dimensional (3-D) mapping of zinc pyrithione (ZnPT) and climbazole (CBZ) deposition detected using confocal Raman imaging (Personal communication Michael Hoptroff, Unilever R&D Port Sunlight, United Kingdom).

Multiphoton[10] fluorescence microscopy is another method that provides cellular resolution and 3-D imaging but requires fluorescent labeling of actives to provide contrast.[11] Antifungals used to treat dermal conditions tend to have smaller molecular weight (MW) than most flourophores and labeling, therefore, radically modifies their physicochemical properties and hence their interaction with the skin surface. In contrast, imaging techniques based on vibrational spectroscopy can be used to provide label-free chemical contrast of compounds derived from the specific vibrational frequency of molecular bonds. However, due to water absorption and the intrinsically low spatial resolution, IR imaging is not applicable to intact skin samples, and the low photon conversion efficiency of Raman (typically lower than 1 in 10^{18} for biological samples) limits its application for confocal 3-D imaging.

Stimulated Raman scattering (SRS) microscopy has recently emerged as a powerful technique that overcomes the low cross-section of Raman scattering through coherent excitation of vibrational modes of interest to provide near real-time, label-free, imaging in intact tissues with 3-D subcellular spatial resolution.[12] A coherent nonlinear Raman signal is generated by focusing two synchronized laser pulse trains (pump and Stokes beams, with frequencies ω_p and ω_S, respectively) onto a sample with their difference in frequency ($\omega_p - \omega_S$) matched to a vibrational mode of a molecular species of interest. The nonlinear nature of this process confines the signal to a submicron diameter focus that can be scanned in 3-D to image chemical species with subcellular resolution. The label-free, quantitative imaging capabilities of the technique have previously proved to be particularly useful for imaging the uptake of analytes into skin[13] and nail.[14]

Using a model system of a formulation of two low-MW antifungal agents with different physicochemical properties applied to *ex vivo* porcine skin, we show that SRS microscopy can be used to provide valuable new insight into the microscopic distribution of AIs on the skin surface. In addition to providing

label-free contrast of the antifungal compounds, SRS can be used to delineate the relevant skin microstructures to determine the physiological location of AIs applied in formulation. Our results demonstrate that SRS provides high-resolution, label-free chemically specific images that reveal the microscopic distribution of two different AIs on the skin surface and their ability to penetrate important structures such as hair follicles.

2 Methods

2.1 *Antifungal Formulation*

To demonstrate that SRS has sufficient sensitivity and chemical specificity to reveal the microscopic locations of AIs with different abilities to penetrate regions of the skin, a model formulation consisting of two antifungal agents with different physicochemical properties was used. CBZ and ZnPT are both low MW (293 and 317, respectively) compounds that are proven to be effective antifungals and are commonly added to commercial shampoo formulations to treat dermal conditions, but each have different modes of action. CBZ is an imidazole with potent antifungal activity and is believed to block the synthesis of fungal cytoplasmic membrane[15] whereas ZnPT is a coordination complex of zinc that inhibits the division of fungal cells.[16] In addition to providing antifungal properties, CBZ also has an impact on the skin's corneocytes, increasing the expression of the cornified envelope, which is in itself beneficial to treating skin conditions.[17]

CBZ and ZnPT have very different hydrophobicity and solubility, which are key factors that affect their ability to penetrate different microscopic chemical environments. Due to the bulky hydrophobic unit ([*p*-chlorphenoxy]3-3dimethyl-2-butanone]), CBZ is significantly more hydrophobic and has a partition coefficient $\log(K_{ow})$ of 3.76 compared with 0.9 for ZnPT. Both compounds have relatively low water solubility, but CLIM is significantly more soluble than ZnPT (50 mg/L compared with 8 mg/L at 20°C), which exists in formulation as a suspension of micron-sized crystals.[18,19]

For studies on porcine skin, model (noncommercial) formulations containing CBZ and ZnPT, each at 3.75%, were prepared in a shampoo base.

2.2 *Stimulated Raman Scattering Microscopy*

SRS microscopy was performed using a picosecond laser system and custom modified commercial laser scanning microscope. Synchronized, dual-wavelength ps excitation was provided by an optical parametric oscillator (OPO) (Levante Emerald, APE-Berlin) synchronously pumped at 532 nm by a frequency-doubled $Nd:YVO_4$ laser (picoTRAIN, high-Q GmB), delivering 6-ps pulses at a repetition rate of 76 MHz. The OPO uses a temperature-tuned noncritically phase-matched LBO crystal to allow continuous tuning of the OPO signal from 690 to 980 nm by adjusting the LBO temperature and an intercavity Lyot filter. The OPO signal and $Nd:YVO_4$

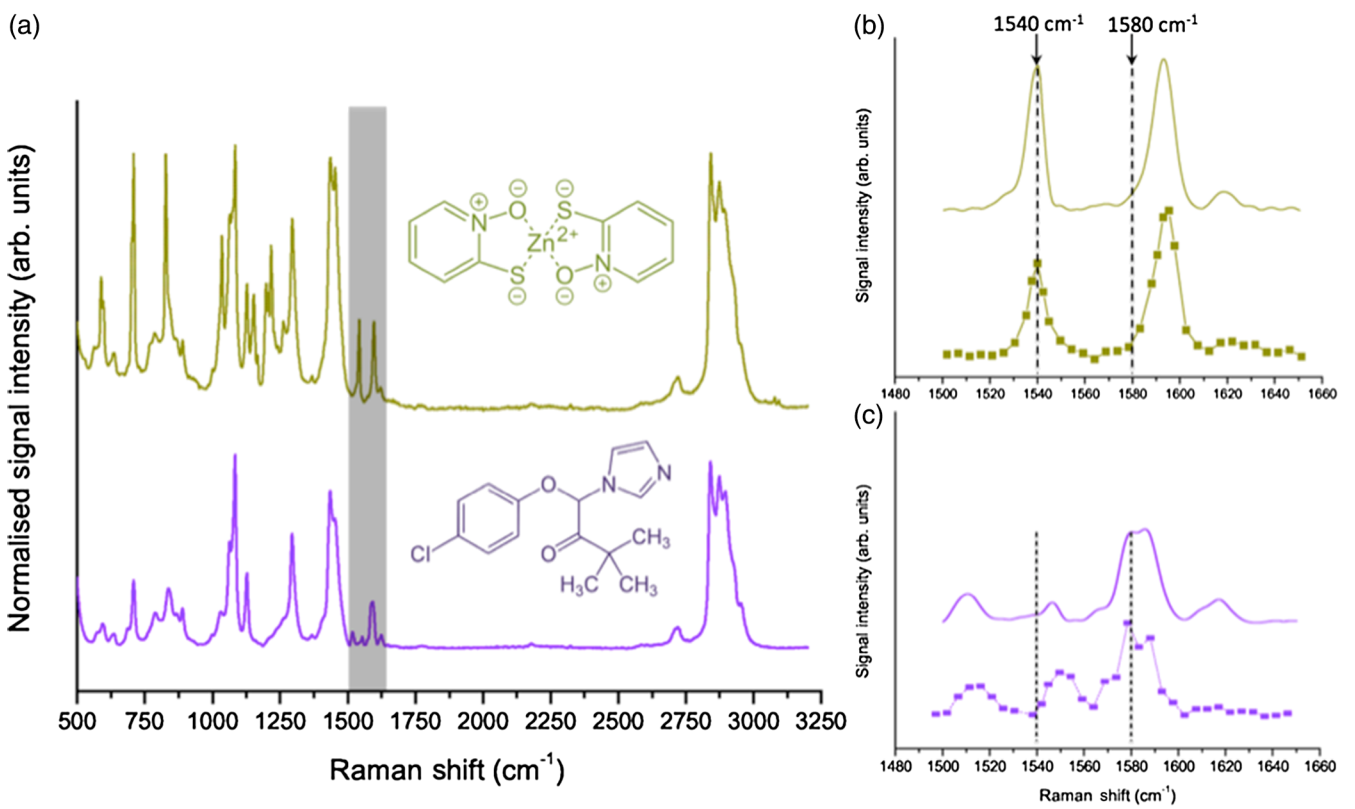

Fig. 2 (a) The normalized spontaneous Raman spectra of CLIM (purple) and ZnPT (yellow) in formulation at a concentration of 1%. The structural formulae of these compounds are shown adjacent to their respective spectra. The highlighted regions in (a) are shown in more detail in (b) ZnPT and (c) CLIM. The solid lines in (b) and (c) correspond to the spontaneous Raman spectra, while the dashed lines correspond to SRS spectra of the same samples. While the spontaneous Raman spectra have been normalized, the SRS spectra in (b) and (c) are presented with the same scale to show the relative signal strengths of the two AIs.

laser fundamental were used at the pump as the Stokes-beams for SRS. The Stokes beam was amplitude modulated at 1.7 MHz using an acousto-optic modulator (AOM 3080-197 Crystal Technology) and spatially overlapped with the pump beam on a dichroic mirror (1064 DCRB, Chroma Technology) and temporal overlapped using a delay-stage.

The collinear beams were directed into the microscope scan unit (FV300/IX71, Olympus UK Ltd., United Kingdom) via a custom port and focused onto the sample using a 1.2 NA water-immersion objective (UPlanSApo, Olympus). SRS was detected in the forward direction by a 1.0 NA condenser lens (LUMFI, Olympus), the Stokes beam was blocked by a bandpass filter (850/90 nm, Chroma), and the pump beam was detected by a large area photodiode (FDS1010, Thorlabs, United Kingdom) positioned at the back-focal plane of the condensing lens. A lock-in amplifier (SR844, Stanford Research Systems) was used to detect the SRS signals with a time constant of 100 μs and images generated by recording the X output.

Spectral SRS acquisition was achieved by sequentially tuning the OPO among image frames. Intensity variations of the OPO signal were corrected by normalizing each data point against the OPO signal intensity, which was recorded with a PIN photodiode. The linear dependence of the SRS signal on the pump beam intensity allows for compensation by straightforward normalization.

2.3 *Spontaneous Raman Scattering Spectroscopy*

Spontaneous Raman spectra were detected using a Renishaw RM1000 Raman microscope (RENISHAW, Wotton-Under-Edge, United Kingdom) equipped with a 1200-line/mm grating providing a spectral resolution of 1 cm^{-1} and a diode laser providing excitation at 785 nm with up to 300 mW power. The system was calibrated prior to every spectral acquisition using the Raman band of a silicon wafer at 520 cm^{-1}. Spectral data were acquired using Renishaw v.1.2 WiRE software. Spectral smoothing and peak analysis were performed using Origin 7.

2.4 *Skin Sample Preparation*

Porcine skin was selected as a model for human skin as it has been shown to exhibit comparable properties to human skin in

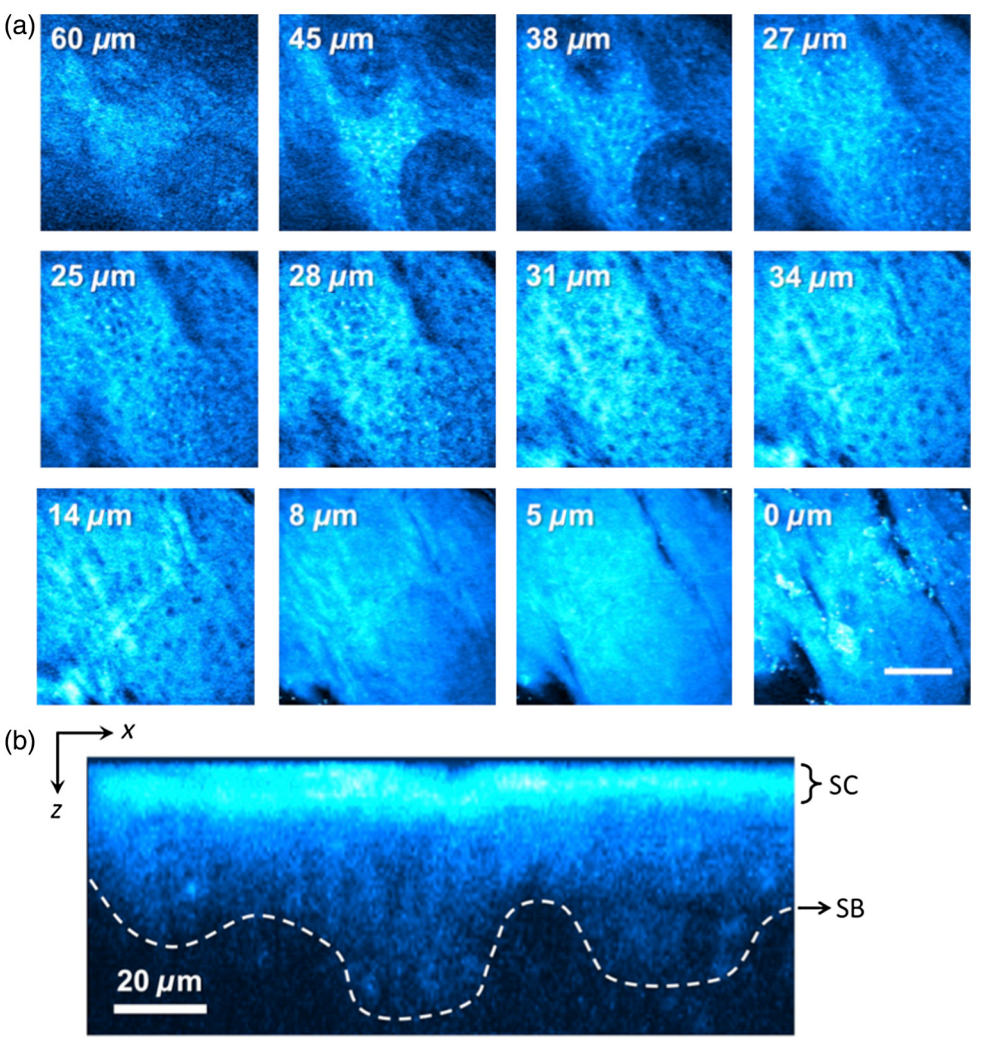

Fig. 3 (a) A series of intensity-corrected *X*-*Y* SRS images taken of untreated porcine skin as a function of depth with the pump and Stokes beams tuned to excite the CH_2 stretch at 2845 cm^{-1}. The *z*-position of each image relative to the surface of the skin is given in each image, and the scale bar is 50 μm. (b) An *X*-*Z* cross-section SRS image of the same sample (without intensity correction) with the location of the SC and SB indicated.

drug penetration studies.[8] To obtain sections of skin of reproducible thickness, a dermatome (Zimmer, Warsaw, Indiana) was used to cut 750-μm-thick sections of fresh porcine abdominal skin from pig carcases that had been slaughtered the same day for food chain purposes. The hairs on the skin were carefully trimmed so as not to damage the delicate SC. The dermatomed skin was cut into smaller regions before being snap-frozen and stored at −20°C. The sections of prepared skin were allowed to thaw at room temperature in a hydrated atmosphere before cut into 1 cm × 1 cm sections prior to experimentation.

Since it is not possible to treat 1 cm × 1 cm skin samples with a wash and rinse application without ensuring that the skin is not exposed to the AI from the underside (which does not present such a tough barrier to AI penetration), the formulations were applied using the following method to mimic the washing procedure. Although this differs from the clinical application (i.e., washing), the AIs are applied in similar (hydrated) conditions. Whilst this a limitation of the experimental procedure, it was necessary to avoid unrepresentative uptake of the AIs via the underside of the skin samples. The porcine skin sections were exposed to antifungal formulations for 15 min in a hydrated atmosphere. Excess topical shampoo formulation was removed from the surface of the skin by gently rolling a clean cotton bud across the skin's surface, prior to the skin being placed on a glass coverslip onto which a 5-μL droplet of phosphate-buffered saline was first placed to ensure good optical contact between the underside of the porcine skin and the glass. A spacer made of three layers of parafilm with a window cut into it was placed around the porcine skin, and a second glass coverslip was placed on top. To provide a water-tight seal, a point heat source was briefly applied to the edges of the glass coverslips to thermally weld the parafilm spacer to the glass. All skin samples were prepared immediately prior to imaging in this manner.

3 Results

Spontaneous Raman spectra of CBZ and ZnPT formulations were acquired to identify unique Raman bands that could be used to distinguish the distribution of each antifungal compound on the skin surface with SRS microscopy. Figure 2(a) shows the spontaneous Raman spectra of CLIM (purple) and ZnPT (yellow) in formulation at a concentration of 1%. The imidazole ring vibration (1580 cm^{-1}) in CLIM and the C=N pyridine stretch (1540 cm^{-1}) in ZnPT were selected since they were unique to each compound and did not overlap with the Raman features of the formulation. The origin of these peaks was confirmed to be from CBZ or ZnPT by comparing Raman spectra of formulations without the two compounds and those of the pure compounds. Figures 2(b) and 2(c) compare SRS spectra obtained by each formulation within the spectral region 1490 to 1650 cm^{-1} with the same region of the spontaneous Raman spectra to confirm that the spectral response of SRS matches that of spontaneous Raman and that the imidazole and C=N pyridine peaks could indeed be resolved with narrow band SRS.

To determine the physiological location of ZnPT and CBZ after topical application onto porcine skin, it was first necessary to obtain surface and cross-sectional SRS images of untreated skin to identify the relevant features. Figure 3 shows selected images from a 3-D SRS data set of the skin. These were acquired with the difference in pump and Stokes frequencies ($\omega_p - \omega_S$) tuned to match the CH_2 stretching frequency at 2845 cm^{-1}. These images illustrate the key structural features of skin as a function of depth below the surface. The intensity of XY images in Fig. 3(a) has been normalized to correct signal attenuation as function of depth. The surface of the SC is uneven, with a flaky appearance. It is devoid of any living cells, being composed primarily of dead, flattened corneocytes. In spite of this, the SRS signal from the SC is very intense when the CH_2 stretch is probed; this is because the dead corneocytes are embedded in a lipid matrix. Past the SC at a depth of ~10 μm below the sample surface, closely packed cells from the stratum lucidum and slightly larger cells of the stratum granulosum are clearly distinguishable. The oval-shaped cell nuclei are darker than the cytoplasm since the nuclei contain more CH_3-rich protein and less CH_2-rich lipid bonds than the cytoplasm. Figure 3(b) shows an example XZ image in which the skin demonstrates that the SC and the undulating stratum basale (SB) can clearly be discerned using the CH_2 stretching mode as contrast.

To confirm that the skin samples did not exhibit SRS signals at wavenumbers used to detect the two compounds (1540 and 1580 cm^{-1}), a number of XYZ data cubes, similar to the example shown in Fig. 2, of control skin samples were obtained at these wavenumbers. The resulting images were found to contain a background signal that was in all samples at least 20 times weaker than the samples treated with the antifungal formulations. The origin of this nonresonant signal is weak nonlinear transient scattering and absorption processes within the skin.[20] The background was sufficiently low that it could be thresholded from the images without causing interference in samples that had been exposed to CBZ and ZnPT.

To investigate how the physicochemical properties of the two antifungal compounds lead to a different microscopic coverage of the surface skin, a formulation containing both CBZ and ZnPT was applied to skin and SRS stacks of the SC. Figure 4 shows a color merged maximum intensity project of three stacks acquired with $\omega_p - \omega_S$ tuned to 1540 cm^{-1} (yellow), 1580 cm^{-1} (purple) and 2845 cm^{-1} (blue) of a hairless region of the SC.

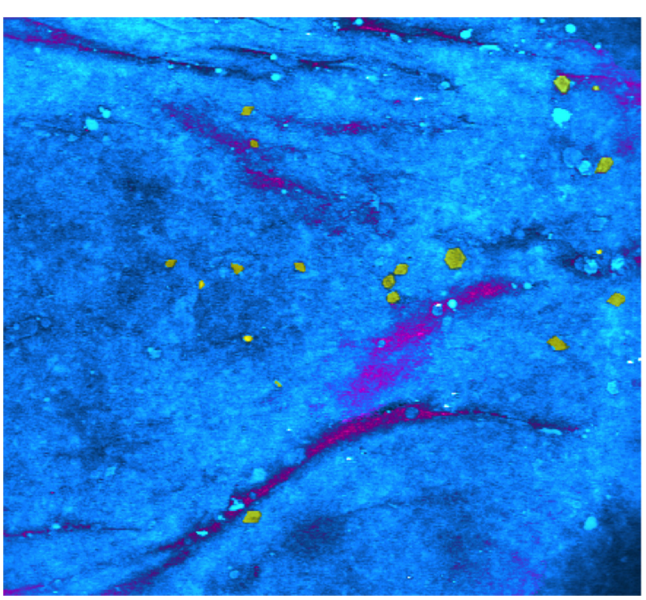

Fig. 4 SRS microscopy image of a sample of porcine skin 1 h after exposure to formulation containing both CLIM and ZnPT. The pump and Stokes beams were tuned to 2845 cm^{-1} to provide contrast of skin lipids (blue), 1540 cm^{-1} for ZnPT (yellow) and 1580 cm^{-1} for CLIM (magenta). The field of view measures 145 μm across.

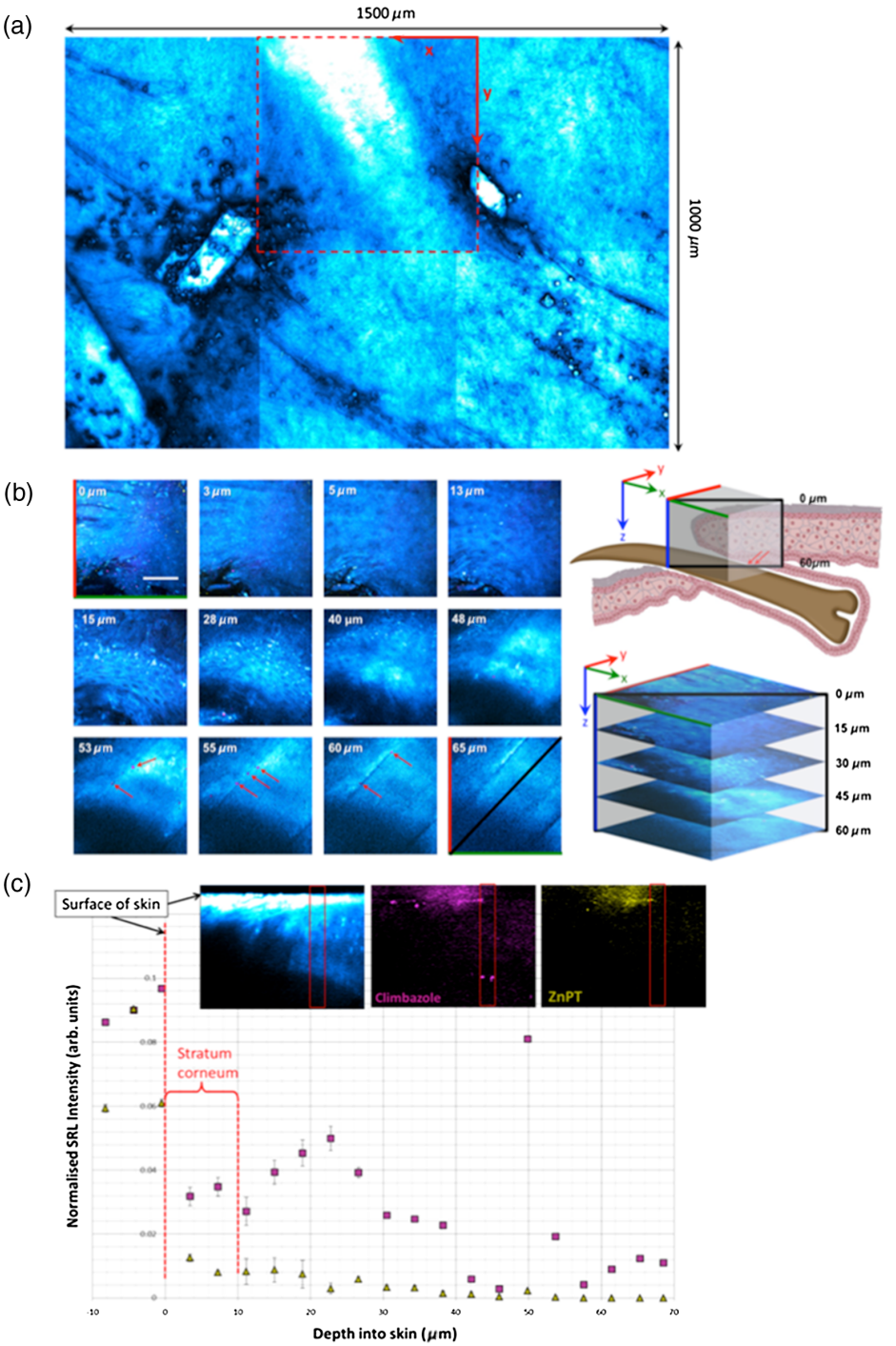

Fig. 5 Penetration of AIs into the infundibular space. Cyan contrast corresponds with signal measured with the pump and Stokes beams tuned to excite the CH-stretch at 2845 cm^{-1}. Magenta contrast arises from CLIM, while yellow contrast was derived from ZnPT, obtained with the pump and Stokes beams tuned to excite 1580 and 1540 cm^{-1}, respectively. (a) A montage of a sequence of *x*-*y* images of a piece of porcine skin covering an area of 1.5 mm × 1 mm. The area indicated with a dashed red box outlines the position of a hair follicle just beginning to emerge from the skin. (b) Left: A series of intensity-corrected *X*-*Y* cross-section SRS images taken of porcine skin 1 h after application of topical foaming cleanser containing 3.75% CLIM and ZnPT. Bottom image: 3-D reconstruction of the same sample (with intensity correction) with the location of the infundibular perimeter marked with a red dashed line. Red arrows mark the positions of the most prominent CLIM signals in this sample. Scale bar is 50 μm. Top right: schematic cross-section through the skin, illustrating the orientation of the hair follicle in the region of interest; the SRS field of view is indicated with a red box, and arrows indicate the position of the Climbazole crystals relative to the hair follicle (not to scale). (c) Penetration profile graph of CLIM (circle) and ZnPT (triangle) as a function of depth (orthogonal to the skin surface rather than along the hair follicle) into porcine skin, measured 1 h after application of the formulation, as determined from SRS microscopy image cubes of a sample of porcine skin containing a hair follicle, measuring 12 μm × 12 μm × 80 μm. The peak in CLIM signal at 50 μm corresponds with the infundibular perimeter of a hair follicle.

It was found that ZnPT was distributed in the form of microcrystals. Analysis of SRS microscopy images in our study shows that the ZnPT particle sizes in this formulation ranged from 1 to 4 μm. In contrast, CBZ was seen to accumulate in microscopic crevasses that accumulate lipids.

In addition to surface coverage, the ability of an antifungal compound to penetrate into the infundibulum of hair follicles is a key factor since these regions are known to harbor fungi and are therefore important target sites for antifungal activity. The typical surface characteristics of the skin are shown in Fig. 5(a), which shows a composite of six 500×500 μm SRS images of the surface of porcine skin acquired with $\omega_P - \omega_S$ tuned to match the CH_2 stretching mode at 2845 cm^{-1}. As shown in Fig. 1, hair follicles grow in infundibular spaces into which oily secretions are channeled via apocrine and sebaceous glands, respectively. The hair shafts do not exit the skin vertically and were found to exit at an angle of 5 deg relative to the surface of the porcine skin. The intense diagonal feature in the image highlighted with the red-dashed border corresponds to a hair follicle just below the SC surface. The notably intense SRS signal at the CH_2 stretching mode corresponds to the oily secretions within the hair follicle.

Figure 5(b) shows a detailed z-stack of the hair follicle highlighted in Fig. 5(a). Regions of CBZ can be seen in purple and the red arrows mark the positions of the most prominent CBZ signals in this sample.

Figure 5(d) shows a graphical comparison of the CBZ and ZnPT signals as a function of depth into the skin in the region of the infundibulum. CBZ is seen to penetrate up to depths of 50 to 60 μm below the skin's surface. ZnPT is seen to penetrate up to depths of 10 to 20 μm below the skin's surface.

4 Discussion

The aim of this study was to determine whether SRS microscopy can offer new capabilities for analyzing the efficacy of antifungal formulations used to treat skin conditions such as dandruff. We have applied the technique to visualize the microscopic distribution of two low MW active ingredients on the surface of *ex vivo* porcine skin treated with antifungal shampoo. In particular, we investigated the ability of SRS to quantify the penetration of ZnPT and CBZ into the interfollicular epidermis and the infundibular space surrounding hair shafts within the epidermis, which is a particularly difficult site to target with existing measurement techniques.

Our results show that SRS has sufficient chemical selectivity and sensitivity to detect the antifungal test compounds on porcine skin surface. The technique, based on their unique chemical motifs that do not occur naturally in biological tissues, maps their distribution with submicron precision. In addition to providing selective contrast of the two antifungal compounds, SRS also revealed the morphological features of the skin using the CH_2 stretch mode, which is abundant in skin lipids. This is a significant strength of the technique since it allows the microscopic accumulation of compounds to be correlated with physiological features and their chemical environment without the use of counter stains. The CH_2 signal can be used to delineate the boundaries among the SC, stratum lucidum, stratum granulosum, stratum spinosum, and the SB. Moreover, we show that the CH_2 contrast can be used to visualize the 3-D structure of hair follicles and to highlight the sebum in the infundibular spaces that surround the upper region of the hair shafts.

Using porcine skin as a model for the human epidermis, we demonstrated that SRS is able to reveal the effect that the physicochemical properties of two test compounds have on their microscopic topographical distribution on the surface of the skin and their ability to penetrate into the hair follicles. Two low MW antifungal compounds (CBZ and ZnPT) have different hydrophobicities and chemical motifs that provided unique vibrational signatures, allowing them to be distinguished from each other and from the cellular structures of skin. We used SRS microscopy to map the surface of the skin at multiple Raman bands corresponding to the two compounds and skin lipids. This mapping highlighted the differences in the surface coverage of the two compounds. Our findings showed that, due to its lower solubility, ZnPT coats the surface of the skin with a sparse layer of crystals in the size range of 1 to 4 μm. This is consistent with the current understanding of the mode of action of ZnPT. Studies investigating the impact of ZnPT particles on the efficacy of topical antifungal formulations show that smaller particles (2.5 μm) are more effective at covering the skin surface than larger particles (12 μm), but they are less able to remain on the skin after rinsing.[21] In contrast, due to being more soluble and hydrophobic, CBZ was observed to predominantly reside in microscopic lipid-rich microfolds[22] and remarkably penetrates up to 60 μm into the infundibular spaces surrounding the hair shaft. ZnPT was observed to penetrate up to 10 to 20 μm. Although it is not possible to rule out the possibility that the AIs are present at concentrations too weak to detect with SRS, our finding demonstrate that a large quantty of the AIs reside on the skin in locations determined by their chemical-physical properties.

Both CBZ and ZnPT are known to be effective antifungal agents and are used as active ingredients in commercial topically applied formulations. The results from this study demonstrate that they target different microscopic regions of the skin. This new information provides evidence to suggest that a combined formulation of CBZ and ZnPT would be more effective in targeting fungal population in both aqueous and lipidic regions of the skin surface. Our results are supported by, and provide mechanistic justification for, clinical observations in which topical treatments containing both CBZ and ZnPT were found to be more effective than treatment by the two compounds independently.[23]

5 Conclusion

In this work, we have shown that SRS enables the distribution of low MW compounds to be mapped on the surface of intact skin with high resolution without the use of extraneous labels. Our results demonstrate that SRS offers significant advantages over current analytical techniques available for studying the treatment of cosmetic skin conditions. The key advantage of SRS over existing techniques used in dermatology is the ability to combine label-free chemically specific compositional analysis with the nondestructive high spatial-resolution imaging capability of optical microscopy. As we have shown, this new capability has the potential to provide new insight into the mechanisms underpinning the topical application of antifungal or skin-active agents that could lead to the rational engineering of enhanced formations.

Disclosures

Authors have no relevant financial interests in the manuscript and no other potential conflicts of interest to disclose.

Acknowledgments

The authors would like to acknowledge financial support from Unilever to undertake all research reported in this manuscript.

References

1. G. A. Turner, M. Hoptroff, and C. R. Harding, "Stratum corneum dysfunction in dandruff," *Int. J. Cosmet. Sci.* **34**(4), 298–306 (2012).
2. T. Schmidt-Rose et al., "Efficacy of a piroctone olamine/climbazol shampoo in comparison with a zinc pyrithione shampoo in subjects with moderate to severe dandruff," *Int. J. Cosmet. Sci.* **33**(3), 276–282 (2011).
3. A. C. Bulmer and G. S. Bulmer, "The antifungal action of dandruff shampoos," *Mycopathologia* **147**(2), 63–65 (1999).
4. R. Chilcott, "Cutaneous anatomy and function," in *Principles and Practice of Skin Toxicology*, R. P. Chilcott and S. Price, Eds., pp. 3–16, John Wiley and Sons, Chichester (2008).
5. M. Ossadnik et al., "Investigation of differences in follicular penetration of particle-and nonparticle-containing emulsions by laser scanning microscopy," *Laser Phys.* **16**(5), 747–750 (2006).
6. B. Lange-Asschenfeldt et al., "Distribution of bacteria in the epidermal layers and hair follicles of the human skin," *Skin Pharmacol. Physiol.* **24**(6), 305–311 (2011).
7. E. Y. M. Bonnist et al., "Understanding the dandruff scalp before and after treatment: an in vivo Raman spectroscopic study," *Int. J. Cosmet. Sci.* **36**(4), 347–354 (2014).
8. C. Herkenne et al., "Pig ear skin ex vivo as a model for in vivo dermatopharmacokinetic studies in man," *Pharm. Res.* **23**(8), 1850–1856 (2006).
9. J. Lademann et al., "Investigation of follicular penetration of topically applied substances," *Skin Pharmacol. Physiol.* **14**(Suppl. 1), 17–22 (2001).
10. G. Chen et al., "Sensitive and simultaneous quantification of zinc pyrithione and climbazole deposition from anti-dandruff shampoos onto human scalp," *J. Chromatogr. B* **1003**, 22–26 (2015).
11. B. Gotter, W. Faubel, and R. H. H. Neubert, "Optical methods for measurements of skin penetration," *Skin Pharmacol. Physiol.* **21**(3), 156–165 (2008).
12. C. W. Freudiger et al., "Label-free biomedical imaging with high sensitivity by stimulated Raman scattering microscopy," *Science* **322**(5909), 1857–1861 (2008).
13. B. G. Saar et al., "Imaging drug delivery to skin with stimulated Raman scattering microscopy," *Mol. Pharm.* **8**(3), 969–975 (2011).
14. W. S. Chiu et al., "Molecular diffusion in the human nail measured by stimulated Raman scattering microscopy," *Proc. Natl. Acad. Sci. U. S. A.* **112**(25), 7725–7730 (2015).
15. M. K. Kathiravan et al., "The biology and chemistry of antifungal agents: a review," *Bioorg. Med. Chem.* **20**(19), 5678–5698 (2012).
16. E. Ermolayeva and D. Sanders, "Mechanism of pyrithione-induced membrane depolarization in Neurospora crassa," *Appl. Environ. Microbiol.* **61**(9), 3385–3390 (1995).
17. J. E. Pople et al., "Climbazole increases expression of cornified envelope proteins in primary keratinocytes," *Int. J. Cosmet. Sci.* **36**(5), 419–426 (2014).
18. E. Richter et al., "Ecotoxicity of climbazole, a fungicide contained in anti-dandruff shampoo," *Environ. Toxicol. Chem.* **32**(12), 2816–2825 (2013).
19. K. V. Thomas, "The environmental fate and behaviour of antifouling paint booster biocides: a review," *J. Biofouling* **17**(1), 73–86 (2001).
20. P. Berto, E. R. Andresen, and H. Rigneault, "Background-free stimulated Raman spectroscopy and microscopy," *Phys. Rev. Lett.* **112**(5), 053905 (2014).
21. J. R. Schwartz, "Product pharmacology and medical actives in achieving therapeutic benefits," *J. Invest. Dermatol. Symp. Proc.* **10**(3), 198–200 (2005).
22. D. M. Drutis et al., "Three-dimensional chemical imaging of skin using stimulated Raman scattering microscopy," *J. Biomed. Opt.* **19**(11), 111604 (2014).
23. G. A. Turner et al., "Enhanced efficacy and sensory properties of an anti-dandruff shampoo containing zinc pyrithione and climbazole," *Int. J. Cosmet. Sci.* **35**(1), 78–83 (2013).

Biographies for the authors are not available.